JOURNAL OF GEOPHYSICAL RESEARCH, VOL. 113, D04302, doi:10.1029/2007JD009021, 2008

Trends, seasonal variability and dominant NO_x source derived from a ten year record of NO_2 measured from space

R. J. van der A,[1] H. J. Eskes,[1] K. F. Boersma,[2] T. P. C. van Noije,[1] M. Van Roozendael,[3] I. De Smedt,[3] D. H. M. U. Peters,[1,4] and E. W. Meijer,[1]

Received 30 May 2007; revised 30 August 2007; accepted 29 November 2007; published 22 February 2008.

[1] For the period 1996–2006, global distributions of tropospheric nitrogen dioxide (NO_2) have been derived from radiances measured with the satellite instruments GOME (Global Ozone Monitoring Experiment) and SCIAMACHY (SCanning Imaging Absorption spectroMeter for Atmospheric CartograpHY). A statistical analysis is applied to derive trends and seasonal variability for this period on a global scale. The time series of the monthly NO_2 columns for these ten years have been fitted with a linear function superposed on an annual seasonal cycle on a grid with a spatial resolution of 1° by 1°. We see significant reductions (up to 7% per year) in NO_2 in Europe and parts of the eastern United States, and a strong increase in Asia, most particularly in China (up to 29% per year) but also in Iran and Russia. By comparing the data with the cloud information derived from the same satellite observations, the contribution of lightning to the total column of NO_2 is estimated. The estimated NO_2 from lightning is, especially in the tropics, in good agreement with lightning flash rate observations from space. The satellite observed seasonal variability of NO_2 generally correlates well with independent observations and estimates of the seasonal cycle of specific NO_x sources. Source categories considered are anthropogenic (fossil fuel and biofuel), biomass burning, soil emissions and lightning. Using the characteristics of the seasonal variability of these source categories, the dominant source of NO_x emissions has been identified on a global scale and on a 1° by 1° grid.

Citation: van der A, R. J., H. J. Eskes, K. F. Boersma, T. P. C. van Noije, M. Van Roozendael, I. De Smedt, D. H. M. U. Peters, and E. W. Meijer (2008), Trends, seasonal variability and dominant NO_x source derived from a ten year record of NO_2 measured from space, *J. Geophys. Res.*, *113*, D04302, doi:10.1029/2007JD009021.

1. Introduction

[2] Nitrogen oxides (NO_x = NO + NO_2) play an important role in atmospheric chemistry. The chemical budget of ozone in the troposphere is largely determined by the concentration of NO_x. NO_x has both substantial anthropogenic sources (e.g., fossil fuel and biofuel combustion and human-induced biomass burning) and natural sources (e.g., soil emissions, wildfires and lightning). Besides NO_x also volatile organic compounds (VOCs) are emitted in large quantities due to human activities such as traffic and industry. In the summer months this mixture of NO_x and VOC often produces photochemical smog. NO_x also chemically reacts to form nitric acid (HNO_3), a major component of acid rain, and nitrate aerosols, acid particles. Through these processes NO_x has a negative effect on crop growth and on health by causing respiratory problems, especially in and near densely populated regions.

[3] To better understand the influence of human activities on the global NO_x budget, we derive the trends in tropospheric NO_2 measured from space over the last 10 years, and we use the observed seasonal variability to categorize the major sources of NO_x.

[4] Global tropospheric NO_2 distributions have been derived from the satellite instruments GOME (1995–2003) aboard ERS-2, SCIAMACHY (from 2002) on the Envisat platform and OMI (Ozone Monitoring Instrument) aboard EOS-AURA (from 2004) [*Leue et al.*, 2001; *Richter and Burrows*, 2002; *Martin et al.*, 2002; *Boersma et al.*, 2004, 2007; *Bucsela et al.*, 2006]. Several comparisons of these NO_2 distributions with ground-based observations have recently been published. In the study of *Petritoli et al.* [2004] and *Schaub et al.* [2006] the tropospheric NO_2 column from SCIAMACHY are compared with in situ and aircraft measurements in the Po Valley and the Alps. In the work of *Blond et al.* [2007] SCIAMACHY measurements are compared with air quality model results and ground measurements. In the study of K. F. Boersma et al., Intercomparison of SCIAMACHY and OMI tropospheric NO_2 columns: Observing the diurnal evolution of chemistry and emissions from space, submitted to *Journal of Geophysical Research*, 2007 the tropospheric NO_2 data of

[1]Royal Netherlands Meteorological Institute, The Netherlands.
[2]Harvard University, USA.
[3]Belgian Institute for Space Aeronomy, Belgium.
[4]Eindhoven University of Technology, The Netherlands.

0148-0227/08/2007JD009021$09.00

SCIAMACHY are compared with observations from the OMI instrument aboard the AURA platform.

[5] Recent studies have used the tropospheric NO_2 satellite measurements for estimating emissions and testing air quality models. *Jaeglé et al.* [2004] used GOME measurements over Africa to map the spatial and seasonal variations of NO_x, mainly caused by biomass burning and soil emissions. *Martin et al.* [2003] used GOME measurements to derive a global *a posteriori* emission inventory. The top-down inventory in combination with a bottom-up emission inventory is used to achieve an optimized posterior estimate of the global NO_x emissions. *Jaeglé et al.* [2005] applied the same approach on GOME measurements, but for sources partitioned into fuel combustion, biomass burning and soil emissions. Different NO_2 retrievals have been systematically intercompared and compared by *van Noije et al.* [2006] with global chemistry transport models. They demonstrated that the top-down emission estimates are sensitive to the choice of model and retrieval. *Boersma et al.* [2005] used GOME measurements to estimate the NO_x production from lightning by comparing modeled and measured spatial and temporal patterns of NO_2 in the tropics.

[6] *Richter et al.* [2005] studied trends in tropospheric NO_2 using a linear regression method, showing especially strong trends over China. A statistical analysis is presented by *van der A et al.* [2006] of the trends in NO_2 over China based on a model, which includes both a linear trend and a seasonal cycle. In this work also the statistical significance of the calculated trend was derived.

[7] Here we analyze the 10-years data set of globally observed tropospheric NO_2 including both the annual trend and the pronounced seasonal cycle, extending our previous analysis which focused on China only. Subsequently, we calculate the statistical significance of the globally derived trends. The seasonal cycle is used to distinguish between the four main sources of NO_x emissions, categorized into (1) fossil fuel (power plants, industry, traffic) and biofuel anthropogenic emissions, (2) biomass burning emissions (man-made or natural), (3) soil emissions, and (4) lightning emissions. From here on we will use the term anthropogenic emissions only for emissions from fossil fuel and biofuel burning.

[8] In this study, for the first time, the different emission sources of NO_x are identified based on satellite observations only.

2. Data Analysis

2.1. Tropospheric NO_2 Retrieval

[9] The GOME and SCIAMACHY satellite spectrometers measure backscattered light from the Earth's atmosphere in the UV and visible wavelength range. GOME NO_2 observations are available since 1995 with a global coverage every 3 days. Since July 2003 a technical failure aboard the ERS platform resulted in a strongly reduced coverage. Since 2002 SCIAMACHY is observing the atmosphere in alternating limb and nadir direction. For tropospheric NO_2 retrievals only the nadir observations are used, resulting in a global coverage every 6 days.

[10] From the observed spectral features around 425–450 nm slant column densities of NO_2 are derived with a Differential Optical Absorption Spectroscopy technique [*Platt*, 1994]. The measured spectrum is fitted with a model, which takes into account the absorption by NO_2, O_3, O_2-O_2 and H_2O, the Ring effect, and describes scattering on clouds, aerosols and air molecules by a low-order polynomial [*Vandaele et al.*, 2005]. This fit results in the total slant column of NO_2 along the path of observation. To derive the tropospheric column thereafter, the following steps are taken. First, the stratospheric part of the NO_2 slant column is deduced by assimilating the slant column data with the TM4 chemistry-transport model driven by meteorological analyses from ECMWF. Subsequently, the analyzed model stratospheric slant column is subtracted from the retrieved slant column, resulting in a tropospheric slant column. The air mass factor (AMF), defined as the ratio between the measured slant column and real vertical column, are used to calculate the tropospheric NO_2 column. The AMFs are derived using pre-calculated radiative transfer calculations with the Doubling-Adding KNMI (DAK) [*Stammes*, 2001] model in combination with TM4 simulated tropospheric NO_2 profile shapes (collocated daily output at overpass time) to correct for the effective photon path length through the atmosphere. The retrieval includes surface albedo values constructed from a combination of the TOMS [*Herman and Celarier*, 1997] and GOME [*Koelemeijer et al.*, 2003] surface reflectivity maps (available on a monthly basis) as described by *Boersma et al.* [2004]. The retrieved NO2 column is a cloud radiance weighted sum of the cloud free and clouded part of the ground pixel. The cloud fraction and cloud top-height are calculated from the same observations with the well-validated FRESCO algorithm [*Koelemeijer et al.*, 2001, *Fournier et al.*, 2006]. *Schaub et al.* [2006, 2007] showed that the NO_2 columns, retrieved with the method described above, under all cloud conditions are in good agreement with their ground observations in Central Europe.

[11] The final NO_2 data product is publicly available on the TEMIS project website (www.temis.nl) with detailed error estimates and kernel information [*Eskes and Boersma*, 2003]. More details on the retrieval are discussed *Boersma et al.* [2004]. As an example of the retrieved tropospheric NO_2, we show in Figure 1 the average over the year 2004.

[12] For our trend and seasonal variability analyses, only the observations with a radiance reflectance of less than 50% from clouds are used. This corresponds to a cloud fraction of less than about 20%. For analyzing the contributions from lightning, we focus on the cloudy pixels instead.

2.2. Time Series Analysis

[13] The GOME data from March 1996 till March 2003 and the SCIAMACHY data from April 2003 till November 2005 have been used to analyze the trends and variability in NO_2. The retrieved tropospheric NO_2 columns are mapped on a 1° by 1° grid, using weighting factors for the overlap between satellite pixel and grid cell. For GOME the ground pixel size is 320 by 40 km^2 (in respectively longitudinal and latitudinal direction), while the ground pixel of SCIAMACHY depends on the solar zenith angle and usually is not larger than 60 by 30 km^2. To have a consistent data set, the gridded monthly mean data of SCIAMACHY is down-graded to a lower resolution by a convolution over 3 grid cells (about 300 km) in

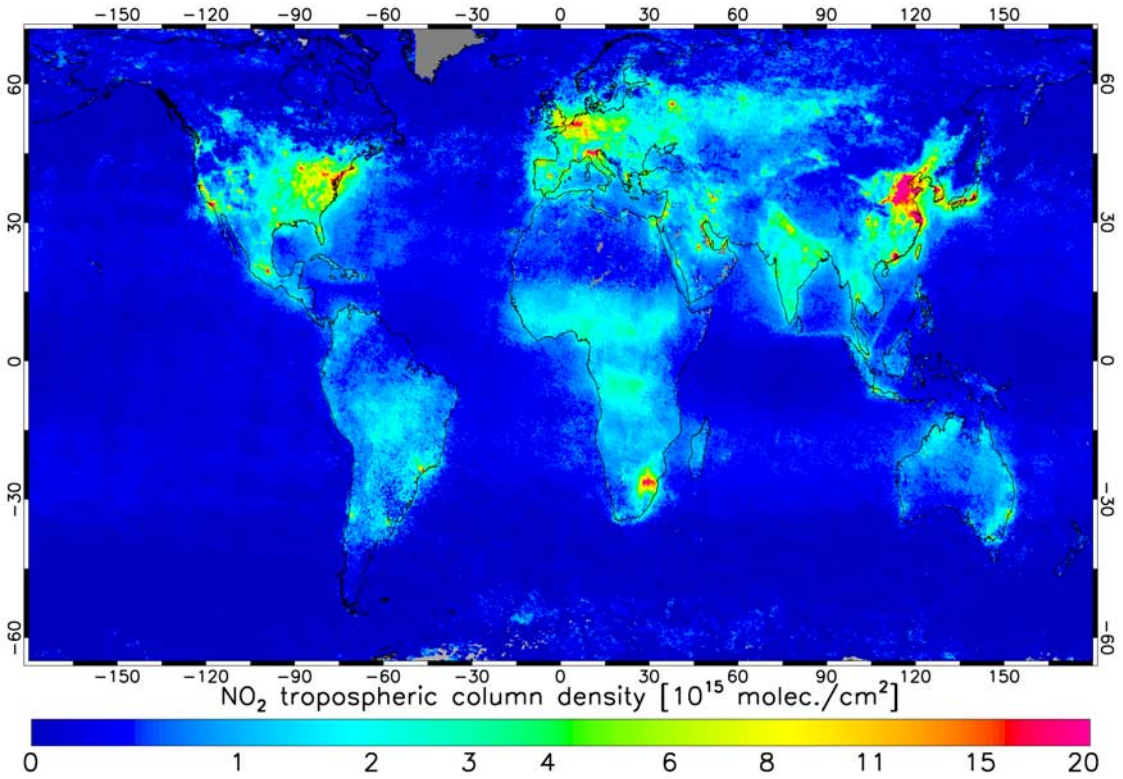

Figure 1. The mean tropospheric NO_2 column for the year 2004 as derived from cloud-free and nearly cloud-free (cloud radiance <50%) SCIAMACHY observations. For the grey areas no observations are shown due to a persistent snow covered ground surface or cloud cover.

the longitudinal direction. The local overpass time of GOME (10.30 am) and SCIAMACHY (10.00 am) is close enough to avoid systematic differences in their time series. In the work of *Richter et al.* [2005] and *van der A et al.* [2006] it was shown that the bias between both data sets is smaller than the minimum error (0.5 10^{15} molec.cm^{-2}) in the data and, therefore, the bias is neglected.

[14] We follow here the analysis method as described by *van der A et al.* [2006]. The time series of NO_2 is represented by the function

$$Y_t = C + \frac{1}{12}BX_t + A\sin(\omega X_t + \alpha) + N_t, \qquad (1)$$

where Y_t represents the monthly mean NO_2 column of month t, X_t is the number of months after January 1996, N_t is the remainder (residual unexplained by the fit function), and C, B, A, and α are the fit parameters. Parameter C is a constant resulting from the fit, and B is the annual trend in NO_2. The seasonal component contains an amplitude A, a frequency ω and a phase shift α. The frequency ω was fixed to a period of one year (i.e., $\pi/6$), since this was the minimum periodicity found in the observations. The uncertainty on the monthly mean is determined by taking the sample standard deviation of the mean with a minimum error of about $1{\cdot}10^{15}$ molec/cm^2 as motivated by *van der A et al.* [2006].

[15] We will follow the commonly used decision rule for trend detection that a trend B is real with a 95% confidence level if $|B/\sigma_B| > 2$, where σ_B is the standard deviation of the trend per year [*Weatherhead et al.*, 1998]. Important input for the calculation of σ_B is the derived retrieval error for each observation.

2.3. Chemistry-Transport Modeling

[16] The analysis of the satellite observations will be compared with model calculations. The chemistry-transport model TM [*Dentener et al.*, 2003 and references therein] has been used to calculate the daily NO_2 values at 10.30 am local time for the year 2000. TM is an offline 3-D model driven by assimilated meteorological fields from the European Centre for Medium-Range Weather Forecasts (ECMWF). In this study we have used output from the TM4 model version in the setup of the ACCENT/IPCC '2030 Photocomp' model intercomparison study [*Stevenson et al.*, 2006; *van Noije et al.*, 2006]. The model was run on a horizontal resolution of 3° × 2° with 25 layers in the vertical, using operational forecasts from the ECMWF for the year 2000.

[17] The anthropogenic emissions of NO_x, CO, and non-methane VOC from power generation, industry, traffic and the domestic sector are based on a recent inventory of national emissions from the International Institute for Applied Systems Analysis (IIASA) for the year 2000 [*Cofala et al.*, 2005], distributed according to the Emission Database for Global Atmospheric Research (EDGAR) version 3.2 for the year 1995 [*Olivier and Berdowski*, 2001]. Emissions from international shipping are added by extrapolation of the EDGAR3.2 emissions for 1995, assuming a growth rate of 1.5% per year. The resulting anthropogenic emissions are

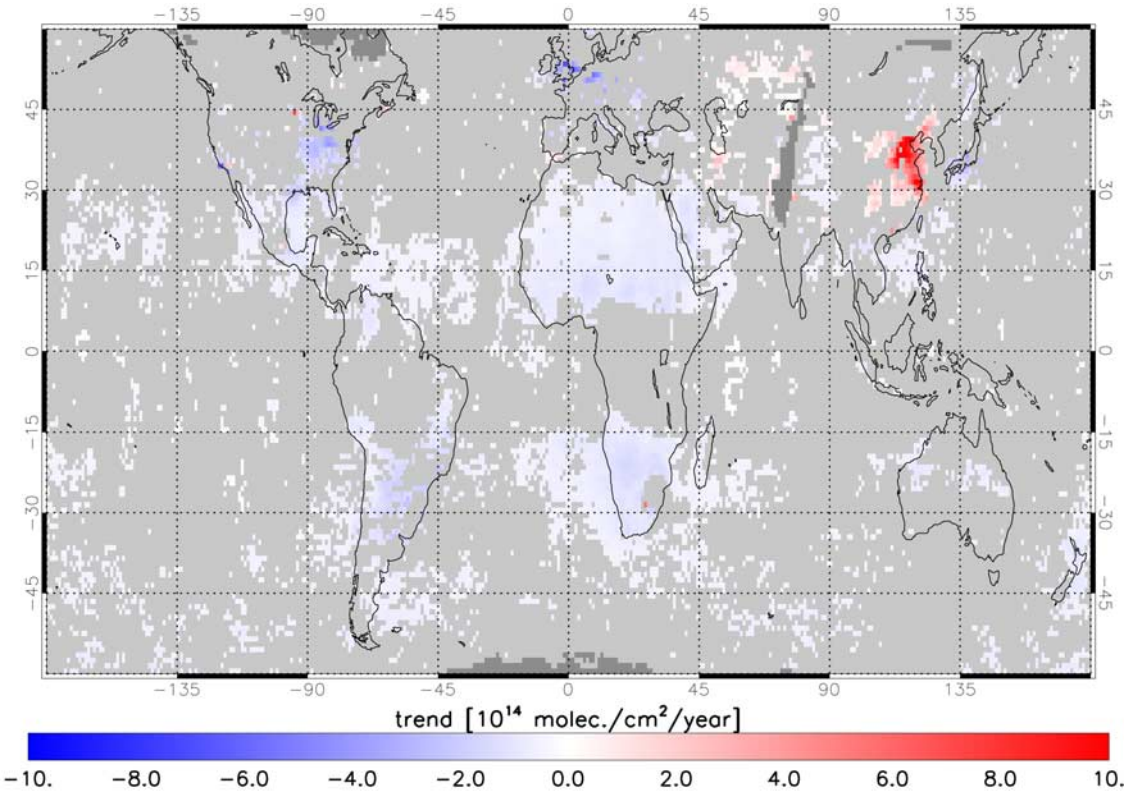

Figure 2. Linear trend per year for tropospheric NO_2 in the period 1996 till 2005 derived from the satellite observation of GOME and SCIAMACHY. For the light grey areas no significant trend has been found in the time series. For the dark grey areas not enough observations were available to construct a time series of tropospheric NO_2.

assumed constant throughout the year. For NO_x they amount to a total of 27.8 Tg N/a.

[18] Emissions from biomass burning are specified on a monthly basis according to the satellite-derived carbon emission estimates from the Global Fire Emissions Database (GFED) version 1 [*van der Werf et al.*, 2003] averaged over the years 1997–2002, in combination with ecosystem dependent emission factors from *Andreae and Merlet* [2001]. To account for fire-induced convection, the biomass burning emissions are released up to a height of 6 km according to an ecosystem dependent vertical distribution [*Dentener et al.*, 2006]. The total amount of NO_x released by biomass burning is 10.1 Tg N/a.

[19] NO_x emissions from aircraft are specified following the ANCAT distribution [*Henderson et al.*, 1999] and amount to 0.79 Tg N for the year 2000. NO_x emissions from soils, which represent natural sources augmented by the use of fertilizers, are based on the parameterization of *Yienger and Levy* [1995], and contribute another 6.0 Tg N/a. Lightning NO_x is modeled using the parameterization of *Meijer et al.* [2001] scaled to an annual total of 7.0 Tg N.

3. Trend Analysis

[20] For all grid cells between −60 and 60 degree latitude, the time series have been fitted with the model described in equation (1), using a non-linear least squares fit that takes into account the calculated retrieval errors. For higher latitudes the time series are usually interrupted in wintertime because NO_2 observations with a high solar zenith angle or a snow/ice covered ground surface are unreliable and, therefore, not used. Figure 2 shows the annual trend B for those grid cells that have a statistically significant trend different from zero (i.e., $|B/\sigma_B| > 2$).

[21] A large positive trend is clearly visible in East China as has been reported by *Richter et al.* [2005] and *van der A et al.* [2006]. Apart from East China there are also regions of increasing NO_2 in India (Delhi, Calcutta), Iran (Tehran and surrounding area), several cities in mid-Russia (e.g., Novosibirsk, Sverdlovsk, Omsk, Celabinsk) and a few spots in central United States and South-Africa. Notable areas of decreasing NO_2 are parts of Europe, the eastern United States and a few spots in California, probably caused by the introduction of cleaner technology. The United States Environmental Protection Agency has mandated stringent emission reduction measures on the electricity producing industry in the eastern U.S. since 1995 [*Frost et al.*, 2006; *Kim et al.*, 2006; K. F. Boersma et al., Validation of OMI tropospheric NO2 observations during INTEX-B and application to constrain NOx emissions over the eastern United States and Mexico, submitted to *Journal of Geophysical Research*, 2007]. However, most of Europe and the USA show no significant trend at all. Another striking issue is the reducing NO_2 associated with biomass burning in southern Africa and northern Argentina. A possible cause is the deforestation in these regions. It should be noted here that these trends are relatively small and although statistically significant they may also have been caused by other factors

Table 1. The Observed Trend for Several Cities in the Period 1996–2006[a]

	Center Coordinates Grid Cell (lat./lon.)	Mean Concentration NO_2 in 1996 [10^{15} molec/cm^2]	Linear Trend in NO_2 [10^{15} molec/cm^2/a]	Annual Growth Rate (%, Reference Year 1996)
		Biggest Megacities		
Tokyo	35.5°/139.5°	10.9	−0.23 ± 0.19	−2.1 ± 2
Mexico City	19.5°/−99.5°	7.5	0.13 ± 0.05	1.7 ± 1
Seoul	37.5°/126.5°	10.4	0.13 ± 0.13	1.3 ± 1
New York	40.5°/−74.5°	12.9	−0.03 ± 0.17	−0.3 ± 1
Sao Paulo	−23.5°/−46.5°	4.9	0.11 ± 0.11	2.2 ± 2
Bombay	18.5°/72.5°	2.3	0.07 ± 0.03	3.0 ± 1
Delhi	28.5°/77.5°	4.1	0.30 ± 0.06	7.4 ± 1
Shanghai	30.5°/121.5°	5.2	1.5 ± 0.24	29 ± 5
Los Angeles	34.5°/−118.5°	11.0	−0.10 ± 0.11	−0.9 ± 1
Osaka	34.5°/135.5°	9.0	0.00 ± 0.11	0.0 ± 1
Jakarta	−6.5°/106.5°	3.7	−0.03 ± 0.04	−0.7 ± 1
Calcutta	22.5°/88.5°	2.6	0.06 ± 0.03	2.2 ± 1
Cairo	30.5°/31.5°	4.0	0.05 ± 0.04	1.3 ± 1
Manila	14.5°/120.5°	2.6	−0.14 ± 0.04	−5.6 ± 1
Karachi	24.5°/67.5°	1.7	0.02 ± 0.02	1.4 ± 1
Moscow	55.5°/37.5°	6.9	0.14 ± 0.27	2.1 ± 4
Buenos Aires	−34.5°/−58.5°	3.3	−0.08 ± 0.06	−2.5 ± 2
Dacca	23.5°/90.5°	2.3	0.03 ± 0.02	1.4 ± 1
Rio de Janeiro	−22.5°/−43.5°	3.8	−0.06 ± 0.07	−1.6 ± 2
Beijing	39.5°/116.5°	11.1	1.2 ± 0.29	11 ± 3
London	51.5°/−0.5°	8.2	0.06 ± 0.17	0.7 ± 2
Tehran	35.5°/51.5°	4.1	0.26 ± 0.05	6.5 ± 1
		Other interesting cities		
Novosibirsk	55.5°/83.5°	1.3	0.13±0.03	11±3
Omsk	54.5°/73.5°	0.84	0.08±0.04	9.9±4
Ruhr (Cologne)	50.5°/6.5°	11.0	−0.40±0.12	−3.6±1

[a]The 22 biggest megacities are ordered by population number.

than decreasing NO_2 emissions. These factors can be changes in surface albedo, aerosol, cloudiness or meteorological conditions over the period of interest, as is discussed by *van der A et al.* [2006]. A combination of these factors may also be responsible for the observed negative trend over the Sahara region.

[22] When comparing these results with the results of *Richter et al.* [2005], where the global trends were shown for 7 years of GOME data using a linear fit without seasonal variation, we see the same patterns with a few exceptions: in China the about 50 % higher trend derived in this study is probably caused by a superlinear (e.g., exponential) growth of NO_2 emissions in China. The extra years (2003–2006) in our fit will therefore increase the trend found in China. Probably for the same reason the significant trend that was found for the densely populated regions in Iran, Russia and Mexico City is not apparent in the results from GOME by Richter et al. Additional differences may be related to differences in the regression and retrieval methods applied in both analyses. Large parts of Europe and the USA, for which a trend was presented by Richter et al., are flagged as not significant in our analysis. On the other hand, the small trend we found for large parts of Africa was not observed by *Richter et al.* [2005].

[23] In Table 1 the observed trend and its error for the period 1996 to 2006 is shown for the 22 largest megacities in the world with more than 10 million citizens. In addition three other large cities with very high trends are in the table. The error on the linear trend contains uncertainties in both the regression model and the measurements. The annual growth, defined as the trend relative to the fitted annual mean in the start year 1996 (third column), is given in the last column as a percentage.

[24] In Table 1 we see that all megacities show high NO_2 concentrations as expected, with the highest NO_2 concentrations in the cities of the economically more advanced countries, e.g., Japan, United States, China, South Korea and Germany. The trends tell another story: the highest trends by far are in the Chinese megacities of Beijing and Shanghai, followed by Delhi, Tehran, and some large cities in Russia, while other megacities with high NO_2 like New York and Tokyo show a small decrease. This seems directly related to the strong economic growth in China as compared to other countries in recent years [see e.g., *Wang et al.*, 2004]. The exact numbers for trends for the Chinese cities differ somewhat from what is reported by *van der A et al.* [2006] because a longer time series has been used for this analysis and the trend in most Chinese cities was found close to exponential, while a linear trend was assumed in the model at forehand.

[25] In regions with the strongest trends the anthropogenic emissions are dominant. Apart from the trend, the fitted parameters also contain information on the seasonal variability that allows identifying the dominant source of emissions in each grid cell, as will be discussed in the next sections.

4. Using Seasonal Variability to Identify NO_2 Sources

4.1. NO_x Sources

[26] In this section we analyze the seasonal cycle of the NO_2 time series. The month in which the seasonal maximum is observed will be compared with model results. Each source of NO_x has specific characteristics that determine its season maximum and variability. We will use these charac-

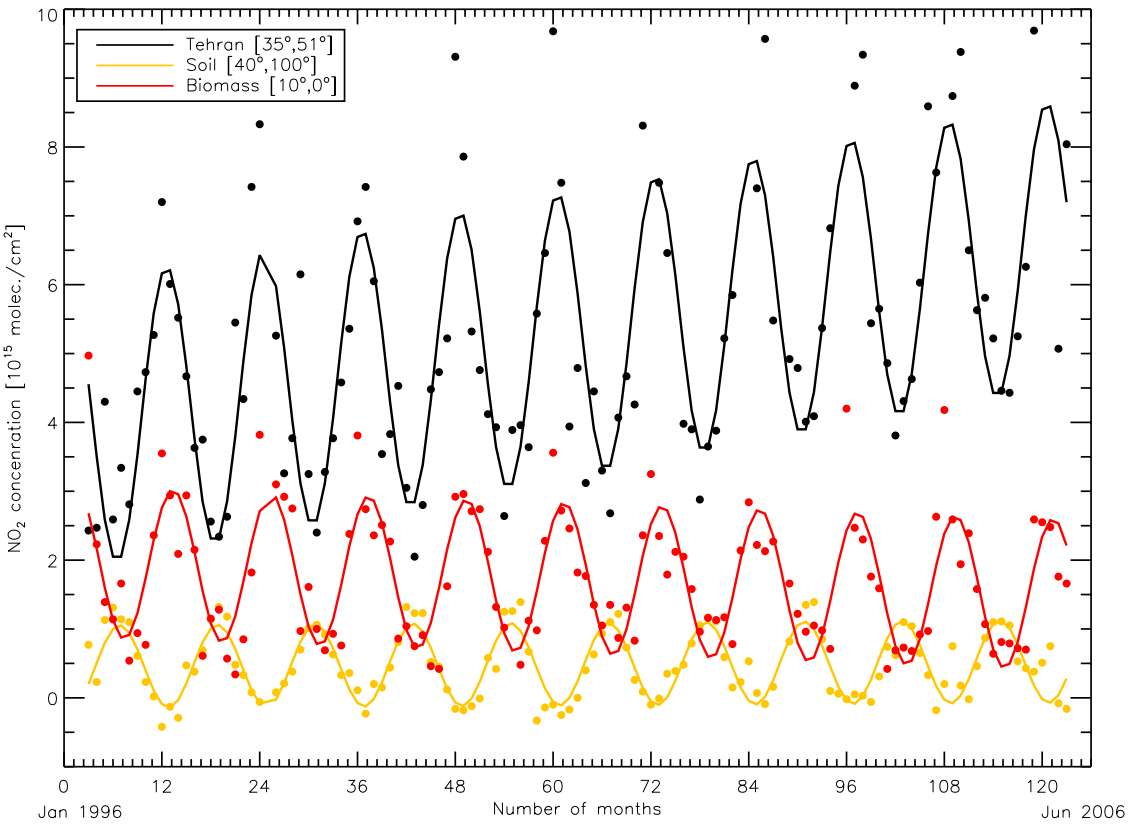

Figure 3. The measured (dots) and fitted (line) time series of NO_2 for three locations, each dominated by a specific NO_x source: anthropogenic (black) for the location of Tehran (35°, 51°), biomass burning (red) for a location (10°, 0°) in Ghana, and soil for a location (40°, 100°) in mid-China.

teristics to identify the dominant source of emissions in each grid cell.

[27] In Figure 3 the measured and fitted time series are shown for three locations, each dominated by a specific NO_x source: anthropogenic, biomass burning and soil. Each NO_x source has its own signature on the annual cycle that is approximated as a sinusoidal function in the regression model. For each grid cell the month of maximum NO_2 is determined by taking the month number that is nearest to $3-6\alpha/\pi$ (for positive A and α in the range $[-19\pi/12, 5\pi/12]$). Figure 4 shows these maxima for the grid cells over land. Only the grid cells with a significant annual cycle are shown, i.e., those grid cells with an amplitude A higher than the error σ_A of the fitted amplitude. Distinct seasonal maxima appear clustered in several large regions, because they share the same dominant NO_2 source.

4.1.1. Anthropogenic

[28] All major industrial regions, Europe, the United States, eastern China, Japan and South Africa, have a seasonal maximum in the winter (December–February on the northern hemisphere, June–August on the southern hemisphere). Exception is the region around the United Kingdom, which is probably strongly affected by meteorological-induced seasonal NO_2 variability. It is also the region with some of the highest fit uncertainties.

[29] Monthly mean values of anthropogenic emissions of NO_x from fuel combustion are relatively constant throughout the year with small variations caused by varying heating and air conditioning [see, e.g., *Jaeglé et al.*, 2005]. However, the resulting tropospheric column of NO_2 will still be higher in winter than in summer due to the changes in the lifetime of NO_x related to changes in the concentration of the hydroxyl radical (OH). In the tropics the lifetime of NO_2 will be determined by the period of wet/dry seasons resulting in a shorter lifetime during the wet season, i.e., the summer time. Therefore the tropospheric column due to anthropogenic emission in the tropics is also expected to show a winter maximum. However, most of the industrial regions are outside the tropics.

4.1.2. Biomass Burning

[30] The burning of biomass is in general the dominant emission source of NO_x in tropical regions. The biomass burning on the African savannas is responsible for one third of the global biomass burning emissions of NO_x [*Cahoon et al.*, 1992]. Biomass burning typically takes place during the dry season, which occurs in the winter and early spring. As shown in Figure 4, the month of maximum NO_2 in Africa moves from January/February in the Sahel region on the Northern Hemisphere to July in the tropical rain forest of Central Africa to October/November in Southern Africa. This correlates well with the movement of the biomass burning season in Africa as observed in the GFED v2 database [*van der Werf et al.*, 2006] and by fire counts [*Arino and Melinotte*, 1999; *Duncan et al.*, 2003] from the AVHRR and ATSR satellites. These observations show that for Africa the peak in

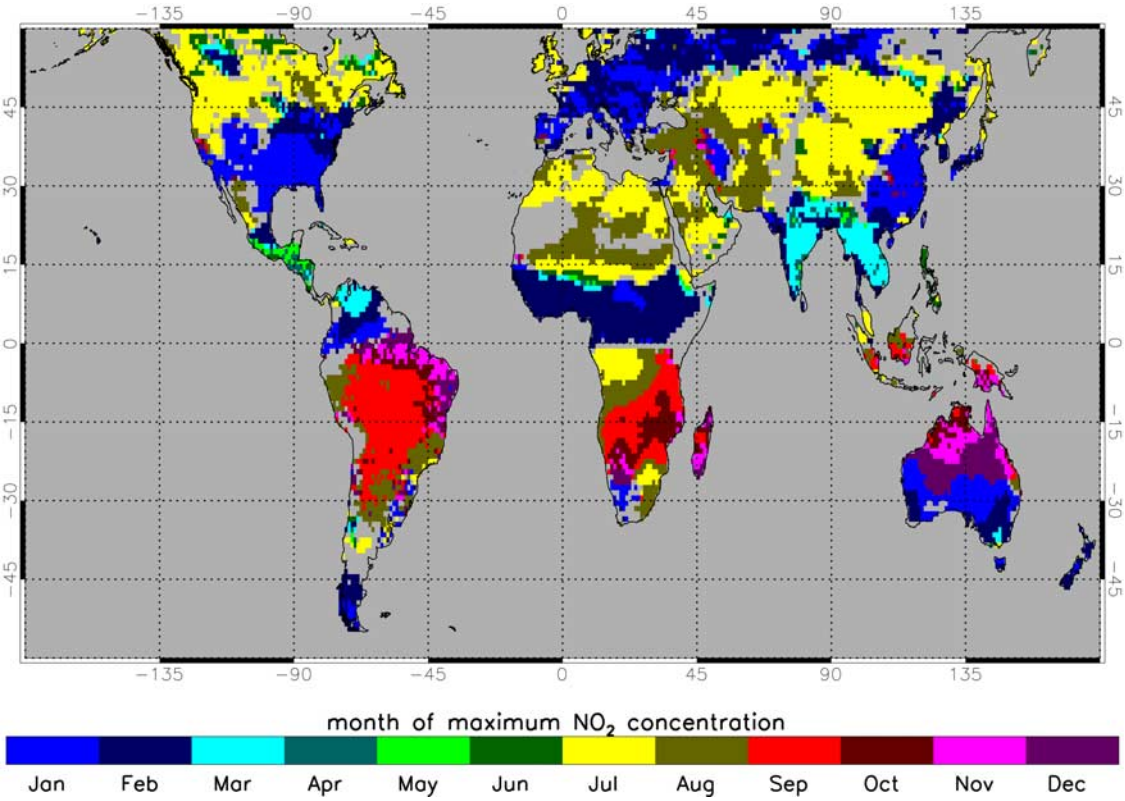

Figure 4. Month of maximum NO_2 for the grid cells over land derived from satellite observations in the period 1996–2006.

the biomass burning season gradually changes from January in the Sahel region on the Northern Hemisphere to June/July just south of the equatorial rain forest and subsequently to August/September in the east and south of Southern Hemisphere Africa. In the months of the wet season almost no fires are observed. Since these months will show very little biomass burning, the relative variability of biomass burning over the year is very high.

4.1.3. Soil

[31] For regions consisting of grassland or sparsely vegetated land, soil emissions of NO_2 can be expected to be the dominant source. *Yienger and Levy* [1995] suggested that soil emissions mainly occur from agricultural ground and grasslands, which contribute to 75% of all soil emissions. Since canopy reduces these emissions, canopy-covered regions like tropical forest show much less NO_2 emissions from the soil. Yienger and Levy showed that the soil NO_x emissions are temperature and moisture dependent. A higher surface temperature leads to higher NO_x emissions in summer time. The summer maximum is augmented by the use of fertilizer [*Bertram et al.*, 2005] and by an effect called ''pulsing'', described by *Yienger and Levy* [1995] and *Jaeglé et al.* [2004] as a sudden increase in NO_x measured after rainfall. From this we infer that soil emissions have a maximum in summertime [*Wang et al.*, 2007]. This is indeed observed in Figure 4 in the grasslands or sparsely vegetated areas of Australia and in the large area spanning the regions from the Sahara, along the Middle East, Central Asia and West China to the tundra in Siberia.

4.2. Model Comparison

[32] To determine the month of maximum NO_2 simulated with the TM4 model, the same sinusoidal function as used to fit the observations has been fitted to the one year of model data. Comparing the modeled phase field (Figure 5) with that observed by the satellite (Figure 4) reveals very similar patterns. However, sometimes the maximum is shifted with about one month. The biggest difference is in the region of Canada with a shift of 2 to 3 months. The observed NO_2 from satellites in this region is very low (0.2×10^{15} molecule/cm^2 on average) and it is plausible that there are small systematic errors that cause deviations in the measured seasonality. Especially the correction for the stratospheric background of NO_2 can show errors of this order of magnitude at these latitudes in wintertime [*Boersma et al.*, 2004]. Besides measurement errors, differences in the comparison may also be caused by an incorrect description of the seasonality in the model. In general, the patterns in the two figures are similar, indicating that the dominant sources of NO_x in both model and observations agree well.

5. Lightning-Produced Emissions

[33] The contribution of lightning to the tropospheric NO_2 column is strongest in the tropics, with a modeled maximum monthly mean of 1.0×10^{15} molec/cm^2 [*Edwards et al.*, 2003] and even lower, an observed maximum of 0.4×10^{15} molec/cm^2 [*Boersma et al.*, 2005], when measuring at 10.30 am. These numbers are substan-

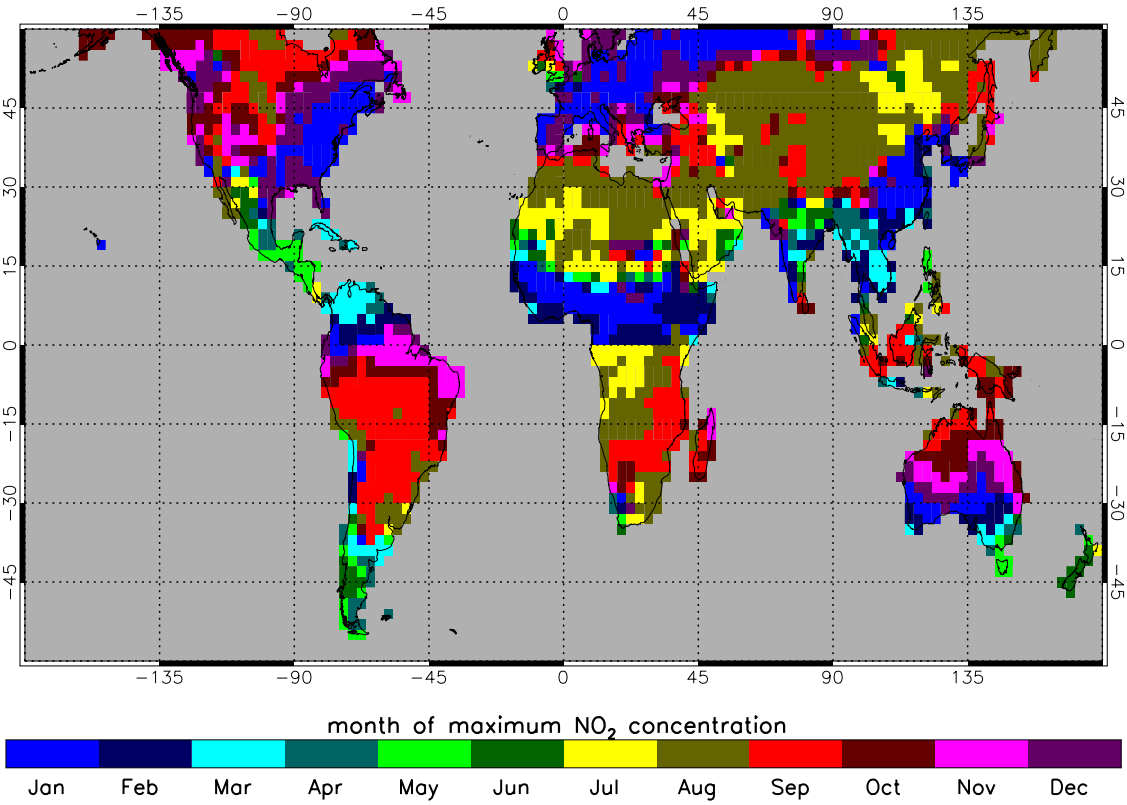

Figure 5. Month of maximum NO_2 concentrations derived from TM4 model results of the year 2000 for the grid cells over land on a resolution of 3 by 2 degrees.

tially smaller than the total observed NO_2 columns over industrialized or biomass burning regions (see Figure 1), so the lightning source will usually be dominated by the other sources discussed above. Therefore we adopt an alternative strategy to identify the contribution of lightning NO_2. Instead of using the cloud-free observations as in the previous section, we focus on the cloud-covered scenes to detect lightning NO_x. The clouds largely hide the NO_2 contributions from sources at the surface, while a substantial fraction of the NO_2 produced by lightning resides at very high altitudes in and above the cloud. Lightning flashes typically occur in high clouds with a cloud top above the 500 hPa level and much of the NO_2 produced is transported to the top of the cloud by the updraft [*Ridley et al.*, 1996; *Skamarock et al.*, 2003; *Pickering et al.*, 1998].

[34] *Boersma et al.* [2005], *Beirle et al.* [2006] and *Martin et al.* [2007] have demonstrated that satellites are able to detect NO_2 produced by lightning over cloudy scenes. On the basis of their analysis of measured above-cloud NO_2 column as a function of cloud height we assume that only pixels with a mean cloud height above 600 hPa in the data set contain lightning-produced NO_2 concentrations. A drawback of this approach is that other emissions of NO_x may also have been uplifted by convection and may show up as above-cloud NO_2. In the tropics where lightning and biomass burning are likely the dominant sources, this is less problematic since these sources generally do not occur simultaneously.

[35] Using the FRESCO cloud retrieval information we selected the set of pixels with a cloud height above the 600 hPa and with a cloud radiance reflectance fraction (CRRF) of more than 75%, similar to the procedure described in *Boersma et al.* [2005]. For pixels with no contribution from other sources in the lower troposphere, the criterion for the CRRF can be relaxed in order to include more partially cloud-covered pixels to reduce the statistical noise. Therefore we adopted the following procedure. For each pixel we compared the three-year average NO_2 column for cases with a CRRF of more than 75% and of more than 50%. If the mean NO_2 column is lower for the CRRF > 50% cases, we assume that for that specific location there are no significant contributions from other sources (which are generally obscured by clouds). For those pixels that satisfy this criterion we use the mean NO_2 column with a CRRF > 50%.

[36] This yields a data set with NO_2 observations that can likely be attributed to lightning without dominant contributions from other sources. In order to estimate the mean amount of lightning NO_2 (as is done for the other sources), the data is weighted by the probability of occurrence of observations with the selected CRRF threshold. Note that this is a conservative estimate, because for instance all lightning NO_2 production above partial cloudy scenes that coincides with strong sources at the surface is excluded. Also all lightning-produced NO_2 at lower altitudes is excluded in this approach. The results of this procedure for 3 years of SCIAMACHY observations are shown in

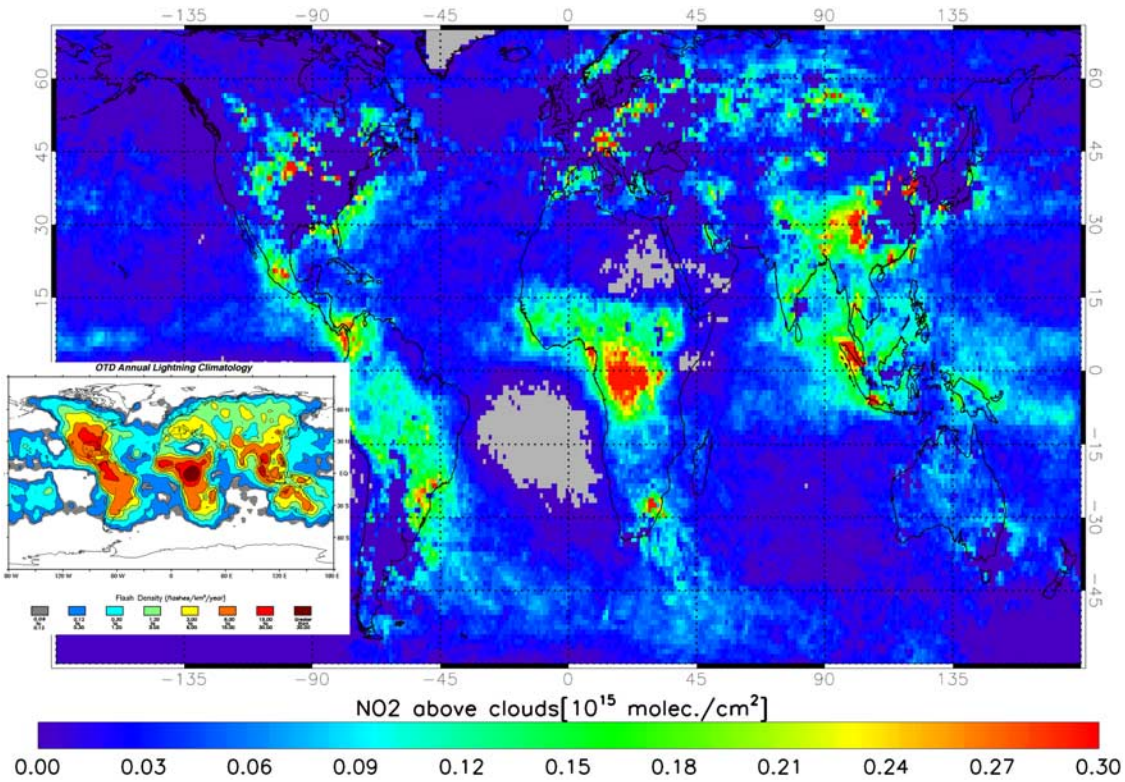

Figure 6. Mean NO_2 column amount at around 10 am local time caused by lightning as measured by SCIAMACHY in the period 2003–2006. The grey area did not have enough observations over high clouds to derive the NO_2 concentration. The inset shows the global distribution of total lightning flash density observed by the OTD (Optical Transient Detector) during September 1995–August 1996.

Figure 6. For comparison an image is added of one year of satellite observations of the OTD (Optical Transient Detector) instrument, which count the number of lightning flashes [*Christian et al.*, 2003; http://thunder.msfc.nasa.gov/].

[37] Figure 6 shows some cases where NO_2 is probably falsely attributed to lightning activity by our simple procedure. This is most clear at southern high latitudes that have hardly any lightning activity. Probably this is caused by transport of pollution in convective systems from South Africa and South America, since lower NO_2 columns for cases with a lower CRRF can also indicate less convective activity if no sources are present at lower altitudes. Furthermore, in South Africa some strong anthropogenic sources occur at the Highveld area, which due to its high altitude is likely the cause of higher NO_2 concentrations in the upper troposphere [*Wenig et al.*, 2003]. Also there are some cases where lightning is detected by the OTD instrument without a NO_2 contribution from lightning by our analysis. This is most clearly seen over the south-east of the US. This is an area where lightning coincides with strong NO_2 sources at the surface.

[38] Despite some difficulties encountered by our method, there is agreement between the lightning NO_2 found with SCIAMACHY and the lightning flashes detected by the OTD instrument. This is especially remarkable given the fact that the diurnal variation of the lightning flash rate over land is very strong with a minimum between 5 and 11 am [*Williams et al.*, 2000; *Boersma et al.*, 2005; *Schuhmann and Huntrieser*, 2007]. The local overpass time of GOME and SCIAMACHY is right at the minimum in the diurnal cycle of lightning flashes over land, while over sea no appreciable diurnal cycle is reported [*Nesbitt and Zipser*, 2003]. The ratio of lightning flashes over land and over sea is estimated to be close to one at the overpass time of GOME (10.30 am) and SCIAMACHY (10.00 am) [*Williams et al.*, 2000]. We find a land-sea ratio of 1.9, in good agreement with the study of Williams et al. and *Boersma et al.* [2005], who found a ratio of 1.6 from GOME observations in 1997.

6. Source Identification

[39] The findings in the previous sections provide us with a simple set of classification rules to identify the dominant source of NO_x for each grid cell. Table 2 lists the decision criteria applied.

[40] The simple criteria in Table 2 are based on the following considerations and assumptions:

Table 2. Decision Scheme for NO_2 Source Identification

	Month of Maximum			
	Northern Hemisphere	Southern Hemisphere	Annual Variability	NO_2(<600 hPa) over NO_2(>600 hPa)
Anthropogenic	Dec–Feb	Jun–Aug	$<V_{max}$	<1.
Biomass burning	Jan–Apr	Jul–Oct	$>V_{max}$	<1.
Soil	Jun–Sept	Dec–Mar	-	<1.
Lightning	-	-	-	>1.

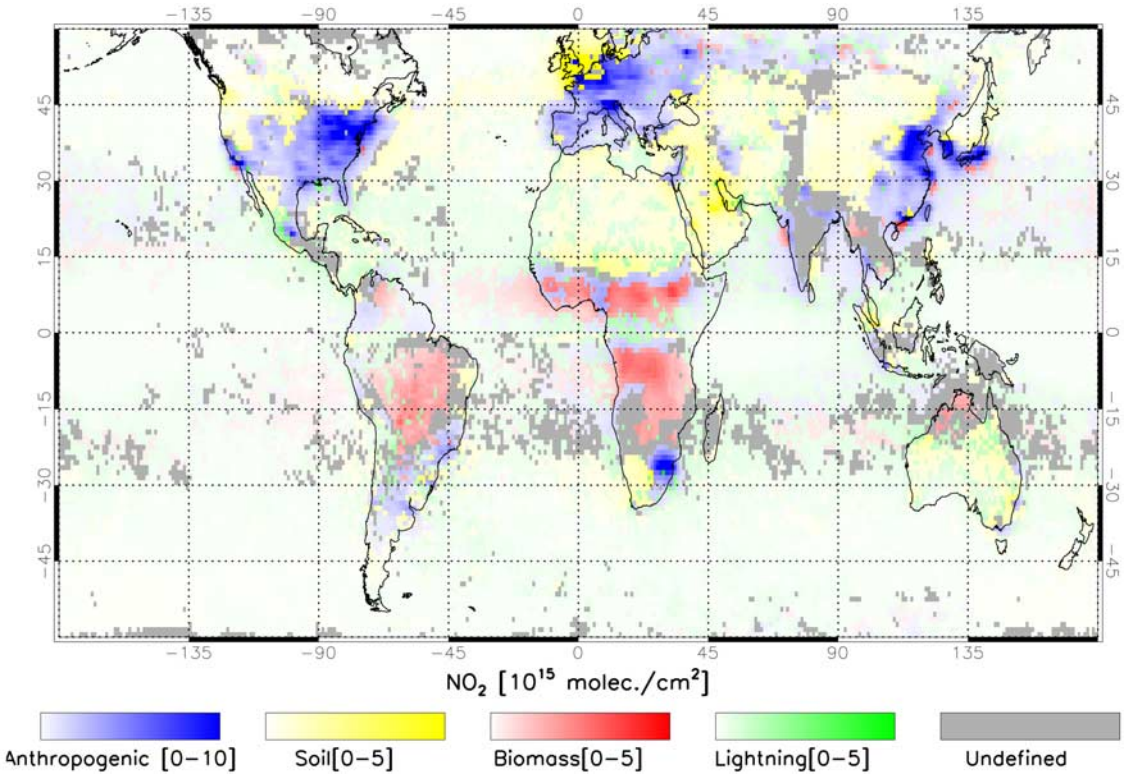

Figure 7. Dominant NO_x source identification based on analyses of the time series of measured tropospheric NO_2 from satellite observations at 10.00 am.

[41] As shown in section 5 a distinction between lightning and other sources can be made by selecting cloudy pixels (with a cloud top pressure below 600 hPa) or cloud-free pixels only. By simply comparing the resulting mean NO_2 column for both cloudy and cloud-free observations at the same location, it is determined whether lightning is the dominant source.

[42] The distinction between NO_2 from soil emissions and from biomass burning or anthropogenic emissions is determined by the month of maximum NO_2. As discussed in section 4, soil emissions typically have their maximum in summer.

[43] To distinguish between the weakly variable anthropogenic NO_2 column (due to relatively constant emissions) (as discussed in section 5) and the highly variable tropospheric NO_2 column caused by biomass burning, we define the annual variability as half the maximum annual variation divided by the annual mean Y_{mean}. Thus from the fit parameters in equation (1) the annual variability is calculated as A/Y_{mean}. The seasonal variation in the lifetime of NO_x depends strongly on the amount of sunlight. To first approximation, it can therefore be assumed that the annual variability of anthropogenic NO_2 is directly related to the variability of the day length, which depends only on latitude and season. The annual variability of anthropogenic NO_2, caused by variations in day length, will only exceed 1 above the polar circle and will be about a half in the tropics. In reality the seasonal cycle in anthropogenic NO_2 is also affected by seasonal variations in anthropogenic emissions and meteorological parameters, but these are assumed to be of secondary importance here. NO_2 from biomass burning is very variable and the annual variability in regions dominated by emissions from biomass burning will usually be close to 1. The limit for distinguishing between anthropogenic and biomass burning emissions is therefore chosen in-between, as a simple polynomial function $V_{max} = 0.5 + 0.5 \cdot (\phi/\phi_{polar})^2$, where ϕ is the latitude of the grid cell and ϕ_{polar} is the latitude of the polar circle (about 66°).

[44] Application of these decision criteria, summarized in Table 2, result in the distribution of the dominant NO_x source as shown in Figure 7. The Figure is in agreement with what is expected on the basis of the locations of populated regions (anthropogenic), grassland (soil emissions) and known biomass burning areas. Interesting to note is also the outflow of anthropogenic NO_2 over the oceans at the East coast of North America and China. Furthermore, outflow of biomass burning NO_2 is visible west of Africa and of Australia. Since the outflow depends on meteorological conditions that have there own seasonality, the identification of outflow is difficult and can easily lead to wrong assignments. This can clearly be seen over the ocean south-east of Japan, where the identified source of biomass burning is unlikely. On land the biomass burning areas are as expected based on fire counts by satellites: mostly in Africa and South America and a region in North-West Australia.

[45] The identification scheme seems to fail over the United Kingdom and the Netherlands. In this region the combination of strong anthropogenic emissions, soil emissions (from fertilized agricultural fields) and the meteorological situation (strong westerly ocean winds) resulted in a less pronounced seasonality that was difficult to fit.

[46] Over the oceans the NO_2 concentration is often very small with large relative uncertainties, which makes the identification less reliable. Apart from the transport from land and some local ship and aircraft emissions, a major, albeit weak source over water is lightning.

[47] A large part of India is undefined because the NO_2 in these grid cells have components of several sources (biomass burning and traffic), while meteorological conditions (notably the monsoon) play an important role in the removal of NO_2. This causes the month of maximum to appear in March just outside our window for anthropogenic sources, while the variability is too low for biomass burning. Still the cities of Delhi, Ahmadabad, Bombay and the heavily populated Ganges valley are clearly visible as dominated by anthropogenic emissions using our classification scheme. Other distinctive isolated spots of anthropogenic emissions are the region around Tehran, the Highveld region in South Africa, and the individual cities of Mexico City, Sao Paulo, Santiago de Chile, Bangkok and Sydney. We calculated that more than half of the total observed tropospheric NO_2 mass has a dominant anthropogenic origin.

7. Conclusions

[48] Ten years of continuous tropospheric NO_2 observations are available from the satellite instruments GOME and SCIAMACHY. With a statistical analysis, trends and their significance are derived for this period on a global scale. Most areas do not show any significant trend or only a small trend. In Asia all trends are positive except for Japan. In China, India and the Asian part of Russia trends of up to 29% per year have been found. Trends are also positive over large cities in Iran and Russia. On the other hand, in Europe the trends are mostly negative, probably as a result of technical measures in automobiles to reduce emissions. In the eastern United States, we also see negative trends, most likely due to reductions in power plant emissions, but in the western part several grid cells with a positive trend have been identified.

[49] The seasonal variability of NO_2 was analyzed, and the observed seasonality is in good agreement with the TM model simulations and fire counts. With a simple classification scheme the dominant source of tropospheric NO_2 is identified, based on the 10-year record of satellite observations.

References

Andreae, M. O., and P. Merlet (2001), Emission of trace gases and aerosols from biomass burning, *Global Biogeochem. Cycles*, *15*(4), 955–966, doi:10.1029/2000GB001382.

Arino, O., and J-M. Melinotte (1999), The 1993 Africa fire map, *Int. J. Remote Sens. Environ.*, *69*, 253–263.

Beirle, S., et al. (2006), Estimating the NOx produced by lightning from GOME and NLDN data: A case study in the Gulf of Mexico, *Atmos. Chem. Phys.*, *6*, 1075–1089, SRef-ID: 1680-7324/acp/2006-6-1075.

Bertram, T. H., A. Heckel, A. Richter, J. P. Burrows, and R. C. Cohen (2005), Satellite measurements of daily variations in soil NOx emissions, *Geophys. Res. Lett.*, *32*, L24812, doi:10.1029/2005GL024640.

Blond, N., K. F. Boersma, H. J. Eskes, R. J. van der A, M. Van Roozendael, I. De Smedt, G. Bergametti, and R. Vautard (2007), Intercomparison of SCIAMACHY nitrogen dioxide observations, in-situ measurements, and air quality modeling results over Western Europe, *J. Geophys. Res.*, *112*, D10311, doi:10.1029/2006JD007277.

Boersma, K. F., H. J. Eskes, and E. J. Brinksma (2004), Error analysis for tropospheric NO_2 retrieval from space, *J. Geophys. Res.*, *109*, D04311, doi:10.1029/2003JD003961.

Boersma, K. F., H. J. Eskes, E. W. Meijer, and H. M. Kelder (2005), Estimates of lightning NO_x production from GOME satellite observations, *Atmos. Chem. Phys.*, *5*, 2311–2331.

Boersma, K. F., et al. (2007), Near-real time retrieval of tropospheric NO2 from OMI, *Atmos. Chem. Phys.*, *7*, 2103–2118.

Bucsela, E. J., E. A. Celarier, M. O. Wenig, J. F. Gleason, J. Veefkind, K. F. Boersma, and E. J. Brinksma (2006), Algorithm for NO_2 vertical column retrieval from the ozone monitoring instrument, *IEEE Trans. Geosci. Remote Sens.*, *44*(4), 1245–1258, doi:10.1109/TGRS.2005.863715.

Cahoon, D. R., Jr., B. J. Stocks, J. S. Levine, W. R. Cofer, and K. P. O'Neill (1992), Seasonal distribution of African savanna fires, *Nature*, *359*, 812–815.

Christian, H. J., et al. (2003), Global frequency and distribution of lightning as observed from space by the Optical Transient Detector, *J. Geophys. Res.*, *108*(D1), 4005, doi:10.1029/2002JD002347.

Cofala, J., M. Amann, R. Mechler (2005), Scenarios of world anthropogenic emissions of air pollutants and methane up to 2030, Report of the Transboundary Air Pollution (TAP) programme, International Institute for Applied Systems Analysis, Laxenburg, Austria.

Dentener, F., W. Peters, M. Krol, M. van Weele, P. Bergamaschi, and J. Lelieveld (2003), Interannual variability and trend of CH4 lifetime as a measure for OH changes in the 1979–1993 time period, *J. Geophys. Res.*, *108*(D15), 4442, doi:10.1029/2002JD002916.

Dentener, F., et al. (2006), Emissions of primary aerosol and precursor gases in the years 2000 and 1750 prescribed data-sets for AeroCom, *Atmos. Chem. Phys.*, *6*, 4321–4344.

Duncan, N. B., R. V. Martin, A. C. Staaudt, R. Yevich, and J. A. Logan (2003), Interannual and seasonal variability of biomass burning emissions constrained by satellite observations, *J. Geophys. Res.*, *108*(D2), 4100, doi:10.1029/2002JD002378.

Edwards, D. P., et al. (2003), Tropospheric ozone over the tropical Atlantic: A satellite perspective, *J. Geophys. Res.*, *108*(D8), 4237, doi:10.1029/2002JD002927.

Eskes, H. J., and K. F. Boersma (2003), Averaging Kernels for DOAS total-column satellite retrievals, *Atmos Chem. Phys.*, *3*, 1285–1291.

Fournier, N., P. Stammes, M. de Graaf, R. van der A, A. Piters, M. Grzegorski, and A. Kokhanovsky (2006), Improving cloud information over deserts from SCIAMACHY Oxygen A-band measurements, *Atmos. Chem. Phys.*, *6*, 163–172.

Frost, G. J., et al. (2006), Effects of changing power plant NO_x emissions on ozone in the eastern United States: Proof of concept, *J. Geophys. Res.*, *111*, D12306, doi:10.1029/2005JD006354.

Henderson, S. C., U. K. Wickrama, et al. (1999), Aircraft emissions: current inventories and future scenarios, in *IPCC Special Report on Aviation and the Global Atmosphere*, eds. J. E. Penner, et al., pp. 290–331, Cambridge University Press, United Kingdom.

Herman, J. R., and E. A. Celarier (1997), Earth surface reflectivity climatology at 340–380 nm from TOMS data, *J. Geophys. Res.*, *102*(D23), 28,003–28,012, doi:10.1029/97JD02074.

Jaeglé, L., R. V. Martin, K. Chance, L. Steinberger, T. P. Kurosu, D. J. Jacob, A. I. Modi, V. Yoboué, L. Sigha-Nkamdjou, and C. Galy-lacaux (2004), Satellite mapping of rain-induced nitric oxide emissions from soils, *J. Geophys. Res.*, *109*, D21310, doi:10.1029/2004JD004787.

Jaeglé, L., L. Steinberger, R. V. Martin, and K. Chance (2005), Global partitioning of NO_x sources using satellite observations: Relative roles of fossil fuel combustion, biomass burning and soil emissions, *Faraday Discuss.*, *130*, 407–423.

Kim, S.-W., A. Heckel, S. A. McKeen, G. J. Frost, E.-Y. Hsie, M. K. Trainer, A. Richter, J. P. Burrows, S. E. Peckham, and G. A. Grell (2006), Satellite-observed U.S. power plant NO_x emission reductions and their impact on air quality, *Geophys. Res. Lett.*, *33*, L22812, doi:10.1029/2006GL027749.

Koelemeijer, R. B. A., P. Stammes, J. W. Hovenier, and J. F. de Haan (2001), A fast method for retrieval of cloud parameters using oxygen A-band measurements from Global Ozone Monitoring Experiment, *J. Geophys. Res.*, *106*, 3475–3490.

Koelemeijer, R. B. A., J. F. de Haan, and P. Stammes (2003), A database of spectral surface reflectivity in the range 335–772 nm derived from 5.5 years of GOME observations, *J. Geophys. Res.*, *108*(D2), 4070, doi:10.1029/2002JD002429.

Leue, C., M. Wenig, T. Wagner, O. Klimm, U. Platt, and B. Jähne (2001), Quantitative analysis of NO_x emissions from Global Ozone Monitoring Experiment satellite image sequences, *J. Geophys. Res.*, *106*, 5493–5505.

Martin, R. V., et al. (2002), An improved retrieval of tropospheric nitrogen dioxide from GOME, *J. Geophys. Res.*, *107*(D20), 4437, doi:10.1029/2001JD001027.

Martin, R. V., D. J. Jacob, K. V. Chance, T. P. Kurosu, P. I. Palmer, and M. J. Evans (2003), Global inventory of nitrogen dioxide emissions

constrained by space-based observations of NO_2 columns, *J. Geophys. Res.*, *108*(D17), 4537, doi:10.1029/2003JD003453.

Martin, R. V., B. Sauvage, I. Folkins, C. E. Sioris, C. Boone, P. Bernath, and J. Ziemke (2007), Space-based constraints on the production of nitric oxide by lightning, *J. Geophys. Res.*, *112*, D09309, doi:10.1029/2006JD007831.

Meijer, E. W., P. F. J. van Velthoven, D. W. Brunner, H. Huntreiser, and H. Kelder (2001), Improvement and evaluation of the parametrisation of nitrogen oxide production by lightning, *Phys. Chem. Earth*, *26*, 577–583.

Nesbitt, S. W., and E. J. Zipser (2003), The diurnal cycle of rainfall and convective intensity according to three years of TRMM Measurements, *J. Clim.*, *16*(10), 1456–1475, doi:10.1175/1520-0442(2003)016.

Olivier, J. G. J., and J. J. M. Berdowski (2001), Global emissions sources and sinks, *The Climate System*, eds. J. J. M. Berdowski, R. Guicherit, and B. J. Heij, pp. 33–78, A. A. Balkema Publishers/Swets & Zeitlinger Publishers, Lisse, The Netherlands.

Petritoli, A., P. Bonasoni, G. Giovanelli, F. Ravegnani, I. Kostadinov, D. Bortoli, A. Weiss, D. Schaub, A. Richter, and F. Fortezza (2004), First comparison between ground-based and satellite-borne measurements of tropospheric nitrogen dioxide in the Po basin, *J. Geophys. Res.*, *109*, D15307, doi:10.1029/2004JD004547.

Pickering, K. E., Y. Wang, W.-K. Tao, C. Price, and J.-F. Müller (1998), Vertical distributions of lightning NO_x for use in regional and global chemical transport models, *J. Geophys. Res.*, *103*(D23), 31,203–31,216, doi:10.1029/98JD02651.

Platt, U. (1994), Differential Optical Absorption Spectroscopy (DOAS), in *Air Monitoring by Spectroscopic Techniques*, *Chem. Anal.*, vol. 127, edited by M. W. Sigrist, pp. 27–76, Wiley-Interscience, Hoboken, N. J.

Richter, A. K., and J. P. Burrows (2002), Tropospheric NO_2 from GOME measurements, *Adv. Space Res.*, *28*, 1673–1683.

Richter, A., J. P. Burrows, H. Nüß, C. Granier, and U. Niemeier (2005), Increase in tropospheric nitrogen dioxide over China observed from space, *Nature*, *437*, 129–132, doi:10.1038/nature04092.

Ridley, B. A., J. E. Dye, J. G. Walega, J. Zheng, F. E. Grahek, and W. Rison (1996), On the production of active nitrogen by thunderstorms over New Mexico, *J. Geophys. Res.*, *101*(D15), 20,985–21,006, doi:10.1029/96JD01706.

Schaub, D., K. F. Boersma, J. W. Kaiser, A. K. Weiss, D. Folini, H. J. Eskes, and B. Buchmann (2006), Comparison of GOME tropospheric NO_2 columns with NO_2 profiles deduced from ground-based in situ measurements, *Atmos. Chem. Phys.*, *6*, 3211–3229.

Schaub, D., K. F. Boersma, J. Keller, D. Folini, D. Brunner, B. Buchmann, H. Berresheim, and J. Staehelin (2007), SCIAMACHY tropospheric NO2 over the Alpine region and importance of pixel surface pressure for the column retrieval, *Atmos. Chem. Phys. Disc.*, *7*, 429–468.

Schuhmann, U., and H. Huntrieser (2007), The global lightning-induced nitrogen oxides source, *Atmos. Chem. Phys. Disc.*, *7*, 2623–2818.

Skamarock, W. C., J. E. Dye, E. Defer, M. C. Barth, J. L. Stith, B. A. Ridley, and K. Baumann (2003), Observational- and modeling-based budget of lightning-produced NO_x in a continental thunderstorm, *J. Geophys. Res.*, *108*(D10), 4305, doi:10.1029/2002JD002163.

Stammes, P. (2001), Spectral radiance modeling in the UV-Visible range, IRS2000: Current problems in atmospheric radiation, edited by W. L. Smith and Y. J. Timofeyev, 385–388, Deepak, A., Hampton, Va, USA.

Stevenson, D. S., et al. (2006), Multi-model ensemble simulations of present-day and near-future tropospheric ozone, *J. Geophys. Res.*, *111*, D08301, doi:10.1029/2005JD006338.

van der A, R. J., D. H. M. U. Peters, H. Eskes, K. F. Boersma, M. Van Roozendael, I. De Smedt, and H. M. Kelder (2006), Detection of the trend and seasonal variation in tropospheric NO_2 over China, *J. Geophys. Res.*, *111*, D12317, doi:10.1029/2005JD006594.

van der Werf, G. R., J. T. Randerson, G. J. Collatz, and L. Giglio (2003), Carbon emissions from fires in tropical and subtropical ecosystems, *Global Change Biology*, *9*, 547–562.

van der Werf, G. R., J. T. Randerson, L. Giglio, G. J. Collatz, and P. S. Kasibhatla (2006), Interannual variability in global biomass burning emission from 1997 to 2004, *Atmos. Chem. Phys.*, *6*, 3423–3441, SRef-ID: 1680-7324/acp/2006-6-3423.

van Noije, T. P. C., H. J. Eskes, F. J. Dentener, D. S. Stevenson, K. Ellingsen, M. G. Schultz, and O. Wild (2006), Multi-model ensemble simulations of tropospheric NO_2 compared with GOME retrievals for the year 2000, *Atmos. Chem. Phys.*, *6*, 2943–2979.

Vandaele, A. C., et al. (2005), An intercomparison campaign of ground-based UV-Visible measurements of NO_2, BrO, and OClO slant columns. I. Methods of analysis and results for NO_2, *J. Geophys. Res.*, *110*, D08305, doi:10.1029/2004JD005423.

Wang, Y. X., M. B. McElroy, T. Wang, and P. I. Palmer (2004), Asian emissions of CO and NO_x: Constraints from aircraft and Chinese station data, *J. Geophys. Res.*, *109*, D24304, doi:10.1029/2004JD005250.

Wang, Y. X., M. B. McElroy, R. V. Martin, D. G. Streets, Q. Zhang, and T. M. Fu (2007), Seasonal variability of NO_x emissions over east China constrained by satellite observations: Implications for combustion and microbial sources, *J. Geophys. Res.*, *112*, D06301, doi:10.1029/2006JD007538.

Weatherhead, E. C., et al. (1998), Factors affecting the detection of trends: Statistical considerations and applications to environmental data, *J. Geophys. Res.*, *103*, 17,149–17,161.

Wenig, M., N. Spichtinger, A. Stohl, G. Held, S. Beirle, T. Wagner, B. Jahne, and U. Platt (2003), Intercontinental transport of nitrogen oxide pollution plumes, *Atmos. Chem. Phys.*, *3*, 387–393.

Williams, E., K. Rothkin, D. Stevenson, and D. Boccippio (2000), Global lightning variations caused by changes in thunderstorm flash rate and by changes in the number of thunderstorms, *J. of Appl. Meteorol.*, *39*, 2223–2230, doi:10.1175/1520-0450(2001)040.

Yienger, J. J., and H. Levy II (1995), Empirical model of global soil-biogenic NO_x emissions, *J. Geophys. Res.*, *100*, 11,447–11,464.

K. F. Boersma, Harvard University, USA.

I. De Smedt and M. Van Roozendael, Belgian Institute for Space Aeronomy, Belgium.

H. J. Eskes, E. W. Meijer, D. H. M. U. Peters, R. J. van der A, and T. P. C. van Noije, Royal Netherlands Meteorological Institute, The Netherlands. (avander@knmi.nl)